Effect of Two Types of Shoulder Prosthesis on the Muscle Forces Using a Generic Multibody Model for Different Arm Motions

Bernhard Weisse (bernhard.weisse@empa.ch)
Swiss Federal Institutes for Materials Testing and Research: Empa Materials Science and Technology
https://orcid.org/0000-0002-5267-5777

Susan Lama
Swiss Federal Institutes for Materials Testing and Research: Empa Materials Science and Technology

Gabor Piskoty
Swiss Federal Institutes for Materials Testing and Research: Empa Materials Science and Technology

Christian Affolter
Swiss Federal Institutes for Materials Testing and Research: Empa Materials Science and Technology

Ameet Krishnan Aiyangar
Swiss Federal Institutes for Materials Testing and Research: Empa Materials Science and Technology

---

Research

Keywords: Reverse shoulder prosthesis, dual-bearing glenoid sparing prosthesis, musculoskeletal model, OpenSim, shoulder biomechanics, muscle activation

Posted Date: May 4th, 2021

DOI: https://doi.org/10.21203/rs.3.rs-477047/v1

Version of Record: A version of this preprint was published at BioMedical Engineering OnLine on March 19th, 2022. See the published version at https://doi.org/10.1186/s12938-022-00988-7.

Abstract

Background: This study aims to analyze the effects of a novel dual-bearing shoulder prosthesis and a conventional reverse shoulder prosthesis on the deltoid and rotator cuff muscle forces for four different arm motions. The dual-bearing prosthesis is a glenoid sparing joint replacement with a moving center of rotation compared to the natural shoulder to increase the moment arms of the acting muscles for arm lifting. It has been developed to treat rotator cuff arthropathy, providing an increased post-operative functionality.

Methods: An OpenSim® three-dimensional musculoskeletal model of an upper body, incorporating a natural gleno-humeral joint and a scapulothoracic joint developed by Blana et al. [1], was used as a reference for the natural shoulder. It was modified by integrating first a novel dual-bearing prosthesis, and second, a reverse shoulder prosthesis into the shoulder joint complex. Four different arm motions, namely abduction, scaption, internal and external rotation, were simulated using an inverse kinematics approach. For each of the three models, shoulder muscle forces and joint reaction forces were calculated with a 2 kg weight in the hand.

Results: In general, the maximal shoulder muscle force and joint reaction force values were in a similar range for both prosthesis models during all four motions. The maximal deltoid muscle forces in the model with the dual-bearing were 18% lower for abduction and 3% higher for scaption compared to the natural shoulder. The maximal rotator cuff muscle forces in the model with the dual-bearing were 36% lower for abduction and 1% higher for scaption compared to the natural shoulder. Although the maximal deltoid muscle forces in the model with the dual-bearing in internal and external rotation were 52% and 64% higher respectively, compared to the natural shoulder, the maximal rotator cuff muscle forces were 27% lower in both motions.

Conclusion: The study shows that the dual-bearing shoulder prosthesis is a feasible option for patients with rotator cuff tear and has a strong potential to be used as secondary as well as primary joint replacement. The study also demonstrates that computer simulations can help to guide the continued optimization of this particular design concept for successful clinical outcomes.

Background

Total shoulder arthroplasty (TSA), classified as Anatomical total shoulder arthroplasty (ATSA) and Reverse total shoulder arthroplasty (RTSA), are predominant in modern shoulder replacement surgery. ATSA involves replacing the gleno-humeral joint with a polyethylene (PE) component fixed to the glenoid and a highly polished metal ball connected to the humerus by a stem, and vice-versa for RTSA. Failure of the polyethylene glenoid component in ATSA including its fixation is the most common impediment [2–4].

In 1985, P. Grammont developed the reverse shoulder prosthesis (RSP) concept that involves the metal ball head fixation in the glenoid cavity and the PE cup in the humerus [5–7]. In RTSA, the medialized

center of rotation (COR) of the gleno-humeral joint increases the deltoid's moment arm by up to 42% and thus reduces deltoid muscle forces in scaption [8, 9]. The worldwide acceptance of RSP shows its efficacy [10]. Today, RTSA is done in all forms of gleno-humeral joint disease with rheumatoid arthritis and serious rotator cuff tears, accounting today more than 40% of the shoulder arthroplasty market [11, 12].

Contemporary RSP designs have not only a medialized but also distalized COR of the gleno-humeral joint compared to conventional RSP to further increase the deltoid's moment arm. Li et al. [13] revealed that this relocated COR is also advantageous for impingement-free motion in internal and external rotations. Hoenecke Jr. et al. [14] postulated that a feasible option is partially medializing the glenosphere, which retains most of the benefits to deltoid efficiency and decreases the risk of scapular notching due to impingement. Several studies found that lateralization of the COR increases the deltoid force in abduction [15–18]. There is a significant amount of literature, which focuses on comparison of optimal RSP placement and designs [19–25]. Liou et al. [11] compared three current RSP designs and found that humeral lateralization optimizes the biomechanics because of its comparatively lower muscle force and increased stability profile based on joint reaction forces (JRF).

There are also some disadvantages of RSA. Potential complications include aseptic loosening, instability, glenosphere dissociation, and scapular notching [6, 12]. Glenoid loosening is the weak link in shoulder replacement, accounting for nearly one third of all TSA complications [26]. Patients affected by these complications have to undergo revision surgeries. For those with a compromised bone stock, no reliable solution is available on the market.

The novel dual-bearing shoulder prosthesis (DBSP) is a joint replacement developed by the Swiss company *41hemiverse AG*. The functionality of this prosthesis is described in the next section. One major advantage is that the surgery required for this prosthesis is less invasive compared to the classical shoulder prosthesis. The proximal component does not need a fixation to the glenoid, which represents a benefit for patients with compromised bone stock, especially at revision surgery. Further benefits of this prosthesis include surgical simplicity minimizing the number of surgical instruments needed while reducing the intraoperative time and compatibility with established shoulder stem platforms, thus, the DBSP provides a unique solution for the revision of failed TSA.

Several studies have shown the power of 3D dynamic rigid multi-body simulation tools for determining movements and internal loads within the musculoskeletal system. Opensim® is one of the software suited for simulating and predicting muscle forces and contains also a repository of models further developed by research groups worldwide. The software was developed by the National Centers for Biomedical Computing at Stanford University and is an established open source software [27]. Shoulder joints were modelled for several years by different groups using OpenSim®, is a validated tool, and showed promising accuracy of results [1, 11, 14, 25, 28–31]. Therefore, this simulation tool was used to analyze the influence of the DBSP and RSP on the muscle forces and JRF for four different motions. The

main objective of this study was to examine and compare the biomechanical behavior of the two types of prosthesis.

Results

Four different motions: (1) ABD (0°-120°); (2) SCP (0°-120°); (3) IR (0°-40°); and (4) ER (40°-0°), were studied for each of the three musculoskeletal models: NS, DBSP, and RSP model. IR motion had starting positon of 60° of forward flexion as shown in Fig. 6. In *Table I*, peak muscle forces and maximal JRF values were noted for each motion for all the three models. *Table II* also shows the percentage change of forces for each muscle group for the two models with prosthesis compared to the NS model. Peak muscle activation was also reported for each group of muscles. Muscle activation definition is given in the muscle activation section.

Muscle forces for the different motions

Abduction (ABD)

In *Table I* the peak muscle forces and peak JRF are reported for the three models. Peak muscle force in the anterior deltoid and posterior deltoid were lower in DBSP model compared to NS and RSP model, but higher in the DBSP for the middle deltoid. The RSP reduced the peak muscle force by 174 N (52.6%) in posterior deltoid compared to the NS model. DBSP reduced the peak muscle force by 222 N (67.3%) in posterior deltoid compared to the NS model. DBSP increased the peak middle deltoid muscle force by 104 N (35.7%) compared to the NS.

The DBSP model also exhibited lower peak force values for rotator cuff muscles compared to the RSP model, although they were higher compared to the NS model. The DBSP increased the peak muscle force by 35 N and 32 N for infraspinatus and teres minor muscles respectively compared to the NS whereas the RSP increased the same muscle forces by 57 N and 81 N respectively. DBSP reduced the peak subscapularis muscle force by 155 N (72.6%) compared to the NS.

Scaption (SCP)

The peak muscle force was 15% higher in anterior deltoid for both RSP and DBSP model compared to the NS model (*Table I*). The peak middle deltoid force increased by 143 N and the peak posterior deltoid force decreased by 145 N for DBSP compared to the NS model. The peak middle deltoid force increased by 38 N and the peak posterior deltoid force decreased by 87 N for the RSP model compared to the NS model.

Table I: Maximal muscle forces and peak joint reaction forces (JRF) in different ranges of motion for the natural shoulder model, the reverse shoulder prosthesis model and the dual-bearing shoulder prosthesis model; ABD: Abduction, SCP: Scaption (SCP), IR: Internal rotation, ER: External rotation.

As shown in *Table I*, peak muscle forces for the DBSP is lower in rotator cuff muscles compared to the RSP. The peak muscle force increases by 39 N, and 42 N for the DBSP in the infraspinatus and teres

minor muscles respectively in comparison to the NS. The peak muscle force increased by 35 N, and 101 N for the RSP in infraspinatus and teres minor muscles respectively in comparison to NS.

Internal rotation (IR)

For IR, both the DBSP and the RSP showed an increase in peak force for the deltoid muscles relative to the NS (*Table I*). The notable increase of 90 N and 120 N in the middle deltoid muscle for the RSP and the DBSP, respectively, compared to the NS was calculated. The RSP showed lower infraspinatus muscle force compared to the DBSP, while the RSP showed higher teres minor and subscapularis muscle force compared to the DBSP.

External rotation (ER)

For ER, the peak muscle force was higher for both the RSP and the DBSP compared to the NS for all deltoid muscles with an exception of the lower force in the anterior deltoid muscle for the RSP as shown in *Table I*. The notable increase was 135 N and 152 N in the middle deltoid muscle for the RSP and DBSP, respectively, compared to the NS was calculated. The muscle forces were lowest for DBSP in teres minor and subscapularis muscles. Infraspinatus muscle force was the lowest in the RSP.

Joint reactions forces

Figure 1 shows the peak (maximal) joint reactions forces (JRF) in the gleno-humeral articulation for the NS, the RSP and DBSP models during four different motions. The peak JRF values are also depicted in *Table I*. For ABD, the maximal JRF was highest in the RSP model (1142 N) and the lowest in the DBSP model (957 N). For SCP, the peak JRF was the highest in the RSP model (1177 N) and the lowest in the NS model (1032 N). The peak JRF for IR was the highest in the DBSP model (946 N); followed by negligible 1.1% decrease in the RSP model and 12.5% decrease in the NS model. Similarly, the peak JRF for ER was the highest in the DBSP (982N); followed by 4.8% decrease in RSP model and 20.7% decrease in the NS model.

Muscle activation

Muscle activation is the ratio of actual muscle force to the maximum isometric force that a muscle can generate at 100% effort. Its value lies between 0 and 1 and it implies the amount of relative effort of the muscle element. For each muscle group, the sum of peak forces produced by each muscle element in that group during a particular motion was divided by the sum of maximal isometric forces of those muscle elements to calculate the peak muscle activation.

Table I clearly shows that the muscle activation for all the models during four different motions are below 0.5, implying a moderate effort. It can be seen that the middle deltoid activation for the DBSP model is higher than for the RSP model. However, the activations for the posterior deltoid and rotator cuff muscles are lower for the DBSP model compared to the RSP model. The highest middle deltoid activation for the

DBSP model is 0.33 during ABD. The highest activation for rotator cuff muscles in the RSP model is 0.33 for teres minor group during IR.

Total muscle force in deltoid and rotator cuff vs. motion angles

Abduction (ABD)

Figure 2 shows the resulting deltoid muscle force in respect to the ABD angle (0-120°) for the NS model, the RSP model and the DBSP model. The deltoid muscle force is the sum of muscle forces of all deltoid muscle sub-groups anterior deltoid, middle deltoid, and posterior deltoid. The dual-bearing and the reverse design have similar curve shape and muscle force magnitudes while the NS reveals a lower deltoid muscle force at lower ABD angles (0–35°) and a higher deltoid muscle force at higher ABD angles (45°-120°). NS has the peak deltoid muscle force value of 619 N at approximately 85°. Dual-bearing and reverse design reduce the peak deltoid muscle force during ABD by 112 N and 133 N respectively.

Figure 3 shows the resulting rotator cuff muscle force in respect to the ABD angle for the NS model, the RSP model, and the DBSP model. The rotator cuff muscle force is the sum of the muscle forces of the infraspinatus, supraspinatus, teres minor, and subscapularis. The dual-bearing design has the lowest rotator cuff muscle values over a large range of ABD angle (0-100°). The magnitude of the rotator cuff muscle force of the RSP model is almost the double of the magnitude of the rotator cuff muscle force of the DBSP model during ABD. Within the considered range of ABD angle (0°-120°), the peak rotator cuff muscle force of the NS model is almost the same than those of the DBSP model, but the curve progression is different, reaching a maximum of 240 N at 62° in the NS model.

Scaption (SCP)

Figure 4 shows the deltoid muscle force in respect to the SCP angle (0°-120°) for the NS model, the RSP model, and the DBSP model. For the dual-bearing design, the deltoid muscle force is the highest for angles between 0 and 65° and it is the lowest at angles above 75°. The maximum deltoid force during SCP is 561 N at 105° for the NS model, followed by around 5% decrease in both RSP model at 76° and DBSP model at 52°.

Figure 5 shows the rotator cuff muscle force in respect to the SCP angle for the NS model, the RSP model, and the DBSP model. The rotator cuff muscle force is higher for the NS model up to a SCP angle of 67°, and this force is the highest in the RSP model for SCP angles above 67°. The highest rotator cuff muscle force during SCP is 401 N at 118° for the RSP model, followed by around 20 % decrease in both the NS model at 50° and the DBSP model at 107°.

Discussion

In this study, DBSP provoke the lowest rotator cuff muscle force when compared to the NS and the RSP in ABD (Fig. 3) and SCP (Fig. 5), which indicates that biomechanically, the dual-bearing design is a feasible option for patients suffering from rotator cuff arthropathy. The results confirm the findings from other

studies, that the RSP generates lower deltoid muscle forces by increasing the moment arm during ABD compared to the NS [5, 8, 9]. For the DBSP, the peak deltoid muscle forces were lower in ABD compared to the NS model (Fig. 2), in SCP the peak deltoid muscle force was higher during lower SCP angles (0–70°), but lower during higher SCP angles (70°-120°) compared to the NS and the RSP model (Fig. 4). Overall, the difference in peak values of deltoid muscle forces during ABD and SCP was not substancial between the reverse and dual-bearing designs, which indicates that the dual-bearing prosthesis is a viable option biomechanically for shoulder replacement surgery in future.

The values of the muscle activation reported in *Table I* imply that all of the muscle groups in the three models have generated efforts below 50% of their maximum capacity. Although the middle deltoid forces and the activations for the DBSP model are higher than for the RSP model, the forces and activations for rotator cuff muscles are lower for the DBSP model compared to the RSP model. It can be interpreted that the middle deltoid in the DBSP model bears more load during arm motion to reduce forces in the rotator cuff muscles. This supports the earlier statement that DBSP can be used for the treatment of patients with severe rotator cuff tear.

When comparing the maximal JRF, the values were approximately similar for all the models with the assumption that the connection between the scapula and the glenoid ring of the DBSP was fixed. In reality, the ring is just supported to the glenoid. However, the acromion, coracoid process, and the surrounding muscles limit the motion of the glenoid ring within the shoulder joint complex.

For IR and ER, the peak middle and posterior deltoid muscle forces (*Table I*) were higher than expected in both the DBSP and RSP models compared to the NS model. The DBSP and RSP exhibited lower peak rotator cuff muscle forces than the NS during IR (26.7% and 27.3%) and ER (26.6% and 29.1%).

This study represents a clinically relevant biomechanical comparison between the NS, the DBSP and the RSP models. The basic musculoskeletal shoulder model used in this research is a verified one originally built in SIMM [1], incorporating all involved joints from the shoulder. The gleno-humeral joint, the sternoclavicular joint, the acromioclavicular joint, and the scapulothoracic joint [31]. The considered four shoulder motion planes provide a good representation of activities of daily life for evaluating the effect of the novel prosthesis on the forces of the involved muscles. Furthermore, preliminary tests on cadavers with inserted dual-bearing prostheses revealed good functionality of this novel design without dislocation.

The shortcomings of this investigation are that it is a computer simulation, which predicts the behavior just after implantation and does not consider the effect of healing and muscle relaxation with the time. The changes in muscle tensioning over time may alter the result but it is not considered in the simulation. Second, this study did not take into account patient-specific anatomic differences that may also affect muscle forces and JRF [11]. The study was more focused on comparing the biomechanical behavior of the novel prosthesis with the RSP and the NS and the additional anatomic variances would have gone beyond the scope of this study, and would have reduced the significance of the afore-mentioned results.

With the help of future validation studies and a proper understanding of how to incorporate computer simulation testing in biomechanics, new prostheses and innovative design variants in TSA can be explored and optimized before their use in clinical trials.

Conclusion

This research presents a biomechanical comparison of generic musculoskeletal shoulder models, including a NS model and two models including a shoulder prosthesis. The study shows that the novel dual-bearing shoulder prosthesis can be a genuine option for patients with rotator cuff arthropathy because of its lower rotator cuff muscle forces during all four arm motions compared to the reverse shoulder prosthesis. Peak values of deltoid muscle force for reverse and dual-bearing designs were in a similar range during ABD and SCP. Low peak muscle activation values for anterior, middle and posterior deltoids during the four motions reveals that in all models, the muscles were not investing high effort when holding 2 kg weight in the hand. Ultimately, this study demonstrates that computer simulation is a useful tool to assess the effects of prosthesis design on the biomechanics of the human musculoskeletal system.

Methods

Model of the natural shoulder (NS)

An existing OpenSim® 3D musculoskeletal model of an upper body incorporating the shoulder joint complex with all involved muscles was used as the NS model in this study (Fig. 6). The model was originally built in SIMM (Software for Interactive Musculoskeletal Modeling, Motion Analysis Corporation, Rohnert Park, California, [27]) by Blana et al. [1], using anatomical data from cadaver studies performed by Klein-Breteler et al. [32]. The well-validated generic model represents the right shoulder of an embalmed 57-year-old muscular man with an estimated height of 168 cm [32]. The model is composed of the following 8 rigid parts: head, thorax including spine, right clavicle, right scapula, right humerus, right ulna, right radius, and right hand. It incorporates a gleno-humeral ball-socket joint and a novel scapulothoracic joint plugin developed by Seth et al. [31]. The scapulothoracic joint plugin provides an improved representation of scapular and clavicular kinematics relative to the thorax during arm motion. The ligaments are not included in the model. There are 29 muscle groups comprising a total of 138 muscle elements. Each muscle is assumed as a tensile force-generating element. Muscle forces are calculated based on the Hill muscle model [33]. Major muscle groups consist of the deltoid group and the rotator cuff group. The deltoid group comprises three sub-groups: anterior deltoid (4 muscle elements), middle deltoid (4 muscle elements), and posterior deltoid (7 muscle elements). The rotator cuff group comprises four subgroups: subscapularis (11 muscle elements), infraspinatus (6 muscle elements), teres minor (3 muscle elements) and supraspinatus (4 muscle elements), which is omitted in the models with prosthesis. At insertion of a shoulder prosthesis, the supraspinatus muscle is cut by the surgeon in order to allow the placement of the implant.

To develop the DBSP and RSP models, the gleno-humeral joint in the NS model was replaced by the two types of prosthesis, as described in the next two sections.

Model including the dual-bearing shoulder prosthesis (DBSP)

The novel dual-bearing shoulder prosthesis concept and design is based on two patents [34, 35]. The components of this prosthesis are depicted in Fig. 7. The prosthesis is assembled by four components and is located between the humerus and the glenoid. For easier reference, the parts are designated with letters A - D.

Before being implanted, the ball head (C) is mounted in the PE-bearing (B). Then, the B-C assembly is inserted in the glenoid ring (A). A snap-in system avoids the unlocking between the B and A parts. The offset adapter (D) is then connected to the part C by press fitting and secured with a screw. Finally, the A-B-C-D assembly is fixed to the humerus stem by press fitting and secured with a screw and is supported proximally to the following bodies: medially by the glenoid (lateral region of the scapula, which normally supports the humerus head), superiorly by the acromion and anteriorly by the coracoid. Although A and C parts are made of Cobalt-Chromium (CoCr) alloy, part B of polyethylene, and part D and the humerus stem of Titanium (Ti) alloy, all components are assumed as rigid bodies in the model. Part B has a hinge joint in respect to part A which means that part B rotates about the central axis of part A. Part C is connected to part B with restriction due to the engagement of the ball head protrusion in the groove of part B. Furthermore, part C can also rotate about the central axis of its protrusion. Thus part C has a gimbal joint in respect to B. The scapula-A, C-D and D-humerus stem connections are assumed as welded together (fixed joint) in the model. The fixed joint between scapula and part A allows the analysis of the joint reaction forces (JRF) between scapula and glenoid ring in OpenSim®. In reality, the DBSP does not require glenoid component fixation, it is placed without anchorage. The stabilization is ensured by the muscles.

The prosthesis system possesses two CORs, one of the joint between the PE-bearing (B) and the glenoid ring (A) and the other between the ball head (C) and the PE-bearing (B). Both CORs are offset from each other. The connections between the parts of the prosthesis and between the prosthesis and the skeleton in the dual-bearing model are summarized in Table II.

Table II: Joint type and connections in the dual-bearing model

The components of the implant are produced in different sizes in order to allow a best fit with the patient's anatomy. For this comparative study, the prosthesis with a 55 mm outer diameter of the glenoid ring was chosen with a medium-sized (M) offset adapter. An ellipsoid wrapping surface with principle axes diameters of 75 mm, 75 mm and 28 mm was used in the model to avoid a penetration of the muscles into the DBSP. The wrapping surface provides a virtual deflection support for the middle line of the muscle. In order to wrap the deltoid muscle elements realistically, the diameter of the implant wrap surface was increased by half of the thickness of deltoid muscle elements (estimated to 20 mm). The

glenoid ring was fixed to the glenoid fossa and tilted 10° downwards to the glenoid plane (Fig. 8, left), similar to the RSP.

Model including the reverse shoulder prosthesis (RSP)

Basically, the model is built up from a ball-and-socket joint. The RSP was kept in the recommended position for surgery [14, 36, 37] in the model as shown in Fig. 8 (right). A humeral cup was positioned at a suitable angle to the humeral shaft axis in such a way that the prosthesis and other segments do not interfere each other. A 36-mm-diameter glenosphere of hemispherical shape was placed with its center in the anteroposterior midline of the glenoid face, the inferior edge of the glenoid baseplate in line with the inferior glenoid rim, and the glenosphere overhanging the inferior rim of the glenoid. A spherical wrapping surface with a diameter of 56 mm was used for this implant in the model, again considering the deltoid muscle thickness for realistic wrapping of the deflected muscle.

Simulated motions

For the three models, four shoulder motions were simulated: abduction (ABD), scaption (SCP), internal rotation (IR) and external rotation (ER). The *Inverse Kinematics* (IK) approach was used to derive rotational joint kinematics from anatomical surface marker-based motion capture data of a single subject, named subject S4, from the shoulder movement database available on SimTK.org [38]. The motions of the markers applied on the subject were measured at 100 Hz. The used markers from the motion capture were duplicated as landmarks in the OpenSim® (V 4.0) model. The motion capture data were then used to drive the model in order to replicate the four shoulder motions. The *Static Optimization* (SO) method was applied to obtain muscle forces for individual muscle elements for the given shoulder motion. In the SO method, the muscle forces are resolved by minimizing the sum of squared (or other power) muscle activations [27]. The IK motion results were noisy with sudden acceleration jumps, which resulted in unrealistic constraint violation and therefore, the SO solver failed to solve the equation for the muscle forces. Generally, IK results are filtered before using the SO solver to overcome the afore-mentioned problem. Data filtering could have also altered the marker dataset and the filtered marker positions may differ from the real marker positions. Therefore, in order to achieve convergence of the results, the original kinematic dataset was modified by stretching the time scale by a factor of 1000. In that way, the sudden acceleration jumps/noise present in the data was reduced by the same factor, without the need to filter the original data. Hence, each motion used to calculate muscle forces and JRFs in all the models resembles a quasi-static motion. No inertial forces were considered.

All three models used the same basic set of muscles. The main physical muscle parameters, like the maximum isometric force, optimal fiber length, tendon slack length and the location of the insertion and origin points of the muscles, were taken unchanged from the NS model. Actuators were added to thorax in all the models to better follow the driven motion. Elbow and wrist were kept fixed during the simulations. The supraspinatus muscle was deactivated during simulation on RSP and DBSP models, considering that supraspinatus is usually impaired during surgery.

Besides the self-weight of the body parts, a weight of 2kg rigidly attached to the hand, simulating a held object, was defined for the simulation of the different arm motions in each of the three models.

Validation of the natural shoulder (NS) model

The shoulder joint reaction forces, known also as the contact forces, were calculated for the NS model with 2 kg load in the hand and compared with the in vivo gleno-humeral joint loads measured on patients using an instrumented shoulder prosthesis [39, 40]. The contact forces at 45° ABD angle for the NS model differs by only 8% compared to the results by Bergmann et al.[39].

Besides this, joint reaction forces during ABD and SCP for the Newcastle reverse shoulder model used by Costantini et al. [19] and the reverse shoulder model used in this study were also found in a similar range for different lateral positions of the implant.

Abbreviations

ABD
Abduction
ATSA
Anatomical Total Shoulder Arthroplasty
COR
Center Of Rotation
DBSP
Dual-Bearing Shoulder Prosthesis
ER
External Rotation
IK
Inverse Kinematics
IR
Internal Rotation
JRF
Joint Reaction Force
NS
Natural Shoulder
PE
Polyethylene
RSP
Reverse Shoulder Prosthesis
RTSA
Reverse Total Shoulder Arthroplasty
SCP

Scaption
SO
Static Optimzation
SIMM
Software for Interactive Musculoskeletal Modeling
TSA
Total Shoulder Arthroplasty

Declarations

Ethics approval and consent to participate

Not applicable.

Consent for publication

The authors certify that this paper is original and unpublished and is not being considered for publication elsewhere and if accepted will not be published elsewhere in the same form, in English or in any other language.

Availability of data and materials

Not applicable / The generated models of the current study are available in the OpenSim repository.

Competing interests

We certify that there were no financial and personal relationships with *hemiverse41* or organizations that could inappropriately influence our work.

Funding

Financial support by the Swiss Innovation Promotion Agency *Innosuisse* is gratefully acknowledged.

Authors' contributions

S. Lama, B. Weisse and G. Piskoty were involved (I) in generating the model and defining the boundary conditions and loading/motions scenarios, (II) in the simulations, and (III) in the result evaluation. A. Aiyangar, Ch. Affolter, and B. Weisse were involved (I) in the definition of the approach, (II) in result

evaluating and interpreting, and (III) discussing the results and conclusions. All authors were involved in the preparation of manuscript.

Acknowledgements

This study was carried out in collaboration with *41hemiverse AG*. We gratefully acknowledge the support in modelling of Malavika Harikrishnan and Gabriel Barreto de Oliveira, both engineering students and trainees at Empa in 2016 and 2017, respectively.

Authors' information (optional)

Not applicable.

References

1. Blana D, et al. A musculoskeletal model of the upper extremity for use in the development of neuroprosthetic systems. J Biomech. 2008;41(8):1714–21.
2. Matsen FA 3. Glenoid component failure in total shoulder arthroplasty. J Bone Joint Surg Am. 2008;90(4):885–96. rd, et al, , (.
3. Walch G, Boileau P, Noel E. Shoulder arthroplasty: evolving techniques and indications. Joint Bone Spine. 2010;77(6):501–5.
4. Wirth MA, Rockwood CA Jr. Complications of total shoulder-replacement arthroplasty. J Bone Joint Surg Am. 1996;78(4):603–16.
5. Berliner JL, et al. Biomechanics of reverse total shoulder arthroplasty. J Shoulder Elbow Surg. 2015;24(1):150–60.
6. Nam D, et al. Reverse total shoulder arthroplasty: current concepts, results, and component wear analysis. J Bone Joint Surg Am. 2010;92(Suppl 2):23–35.
7. Sabharwal S, Bale S. The biomechanics of reverse shoulder arthroplasty. Journal of Arthroscopy and Joint Surgery; 2020.
8. Boileau P, et al. Reverse total shoulder arthroplasty after failed rotator cuff surgery. J Shoulder Elbow Surg. 2009;18(4):600–6.
9. Kontaxis A, Johnson GR. The biomechanics of reverse anatomy shoulder replacement–a modelling study. Clin Biomech (Bristol Avon). 2009;24(3):254–60.
10. Sirveaux F, et al. Grammont inverted total shoulder arthroplasty in the treatment of glenohumeral osteoarthritis with massive rupture of the cuff. Results of a multicentre study of 80 shoulders. J Bone Joint Surg Br. 2004;86(3):388–95.
11. Liou W, et al. Effect of lateralized design on muscle and joint reaction forces for reverse shoulder arthroplasty. J Shoulder Elbow Surg. 2017;26(4):564–72.

12. Wall B, et al. Reverse total shoulder arthroplasty: a review of results according to etiology. J Bone Joint Surg Am. 2007;89(7):1476–85.
13. Li X, et al. Effects of glenosphere positioning on impingement-free internal and external rotation after reverse total shoulder arthroplasty. J Shoulder Elbow Surg. 2013;22(6):807–13.
14. Hoenecke HR Jr, Flores-Hernandez C. and D.D. D'Lima, *Reverse total shoulder arthroplasty component center of rotation affects muscle function*. J Shoulder Elbow Surg. 2014;23(8):1128–35.
15. Nolte PC, et al., *The effect of glenosphere lateralization and inferiorization on deltoid force in reverse total shoulder arthroplasty*. J Shoulder Elbow Surg, 2020.
16. Henninger HB, et al. Effect of lateral offset center of rotation in reverse total shoulder arthroplasty: a biomechanical study. J Shoulder Elbow Surg. 2012;21(9):1128–35.
17. Hettrich CM, et al. Mechanical tradeoffs associated with glenosphere lateralization in reverse shoulder arthroplasty. J Shoulder Elbow Surg. 2015;24(11):1774–81.
18. Giles JW, et al. Implant Design Variations in Reverse Total Shoulder Arthroplasty Influence the Required Deltoid Force and Resultant Joint Load. Clin Orthop Relat Res. 2015;473(11):3615–26.
19. Costantini O, et al. The effects of progressive lateralization of the joint center of rotation of reverse total shoulder implants. J Shoulder Elbow Surg. 2015;24(7):1120–8.
20. Hamilton MA, et al. Effect of reverse shoulder design philosophy on muscle moment arms. J Orthop Res. 2015;33(4):605–13.
21. Hamilton MA, et al, *Effect of prosthesis design on muscle length and moment arms in reverse total shoulder arthroplasty.* Bull Hosp Jt Dis (2013), 2013. **71 Suppl 2**: p. S31-5.
22. Langohr GD, et al. Contact mechanics of reverse total shoulder arthroplasty during abduction: the effect of neck-shaft angle, humeral cup depth, and glenosphere diameter. J Shoulder Elbow Surg. 2016;25(4):589–97.
23. Roche CP, et al, *Impact of inferior glenoid tilt, humeral retroversion, bone grafting, and design parameters on muscle length and deltoid wrapping in reverse shoulder arthroplasty.* Bull Hosp Jt Dis (2013), 2013. **71**(4): p. 284 – 93.
24. Walker DR, et al. How do deltoid muscle moment arms change after reverse total shoulder arthroplasty? J Shoulder Elbow Surg. 2016;25(4):581–8.
25. Walker DR, et al. How sensitive is the deltoid moment arm to humeral offset changes with reverse total shoulder arthroplasty? J Shoulder Elbow Surg. 2016;25(6):998–1004.
26. Sircana G, Merolla G, Paladini P. Surgical rationale and controversies of glenoid replacement in osteoarthritis: How to choose the glenoid implant? Journal of Arthroscopy Joint Surgery. 2021;8(1):27–34.
27. University Cf.B.C.a.S., *OpenSim Documentation.* https://simtk-confluence.stanford.edu/display/OpenSim/DocumentationNational 2018.
28. Glenday J, et al. Effect of humeral tray placement on impingement-free range of motion and muscle moment arms in reverse shoulder arthroplasty. Clin Biomech (Bristol Avon). 2019;62:136–43.

29. Sabesan VJ, et al. Does Acromion Anatomy Affect the Risk of Acromion Stress Fracture after Reverse Shoulder Arthroplasty? Seminars in Arthroplasty: JSES; 2020.
30. Shah SS, et al. Influence of implant design and parasagittal acromial morphology on acromial and scapular spine strain after reverse total shoulder arthroplasty: a cadaveric and computer-based biomechanical analysis. J Shoulder Elbow Surg. 2020;29(11):2395–405.
31. Seth A, et al. A Biomechanical Model of the Scapulothoracic Joint to Accurately Capture Scapular Kinematics during Shoulder Movements. PLoS One. 2016;11(1):e0141028.
32. Klein Breteler MD, Spoor CW, Van der Helm FC. Measuring muscle and joint geometry parameters of a shoulder for modeling purposes. J Biomech. 1999;32(11):1191–7.
33. Thelen DG. Adjustment of muscle mechanics model parameters to simulate dynamic contractions in older adults. J Biomech Eng. 2003;125(1):70–7.
34. Overes T, Frigg R. Joint implant. Google Patents; 2018.
35. Overes T, Frigg R. Shoulder prosthesis assembly. Google Patents; 2018.
36. Boileau P, et al. Grammont reverse prosthesis: design, rationale, and biomechanics. J Shoulder Elbow Surg. 2005;14(1 Suppl S):147S–161S.
37. Nyffeler RW, Werner CM, Gerber C. Biomechanical relevance of glenoid component positioning in the reverse Delta III total shoulder prosthesis. J Shoulder Elbow Surg. 2005;14(5):524–8.
38. Model, S.-D.S.a.E., 2018.
39. Bergmann G, et al. In vivo glenohumeral contact forces–measurements in the first patient 7 months postoperatively. J Biomech. 2007;40(10):2139–49.
40. Bergmann G, et al. In vivo gleno-humeral joint loads during forward flexion and abduction. J Biomech. 2011;44(8):1543–52.

Tables

Due to technical limitations, table 1 and 2 is only available as a download in the Supplemental Files section.

Figures

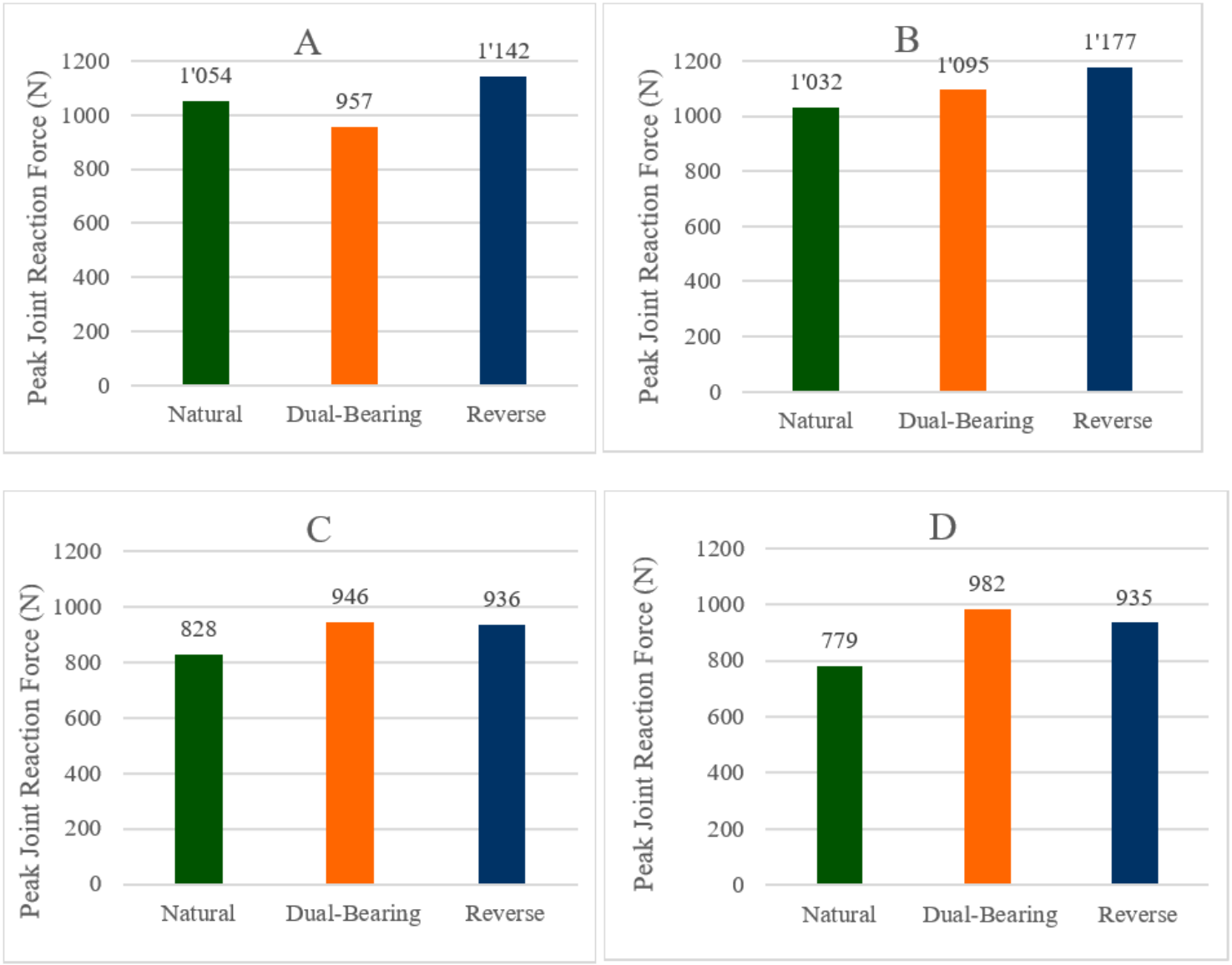

Figure 1

Peak total joint reaction forces for four simulated motions for the natural shoulder, the dual-bearing shoulder and the reverse shoulder prosthesis model. A) Abduction (ABD), B) Scaption (SCP), C) Internal rotation (IR), and D) External rotation (ER).

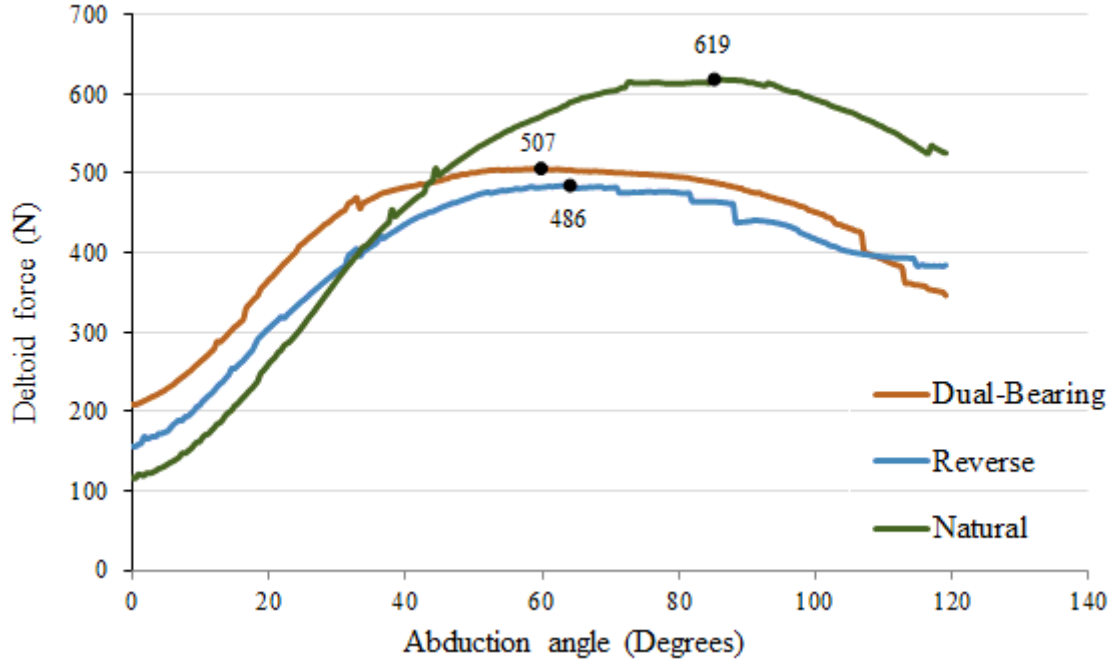

Figure 2

Deltoid muscle force vs abduction (ABD) angle for different shoulder models

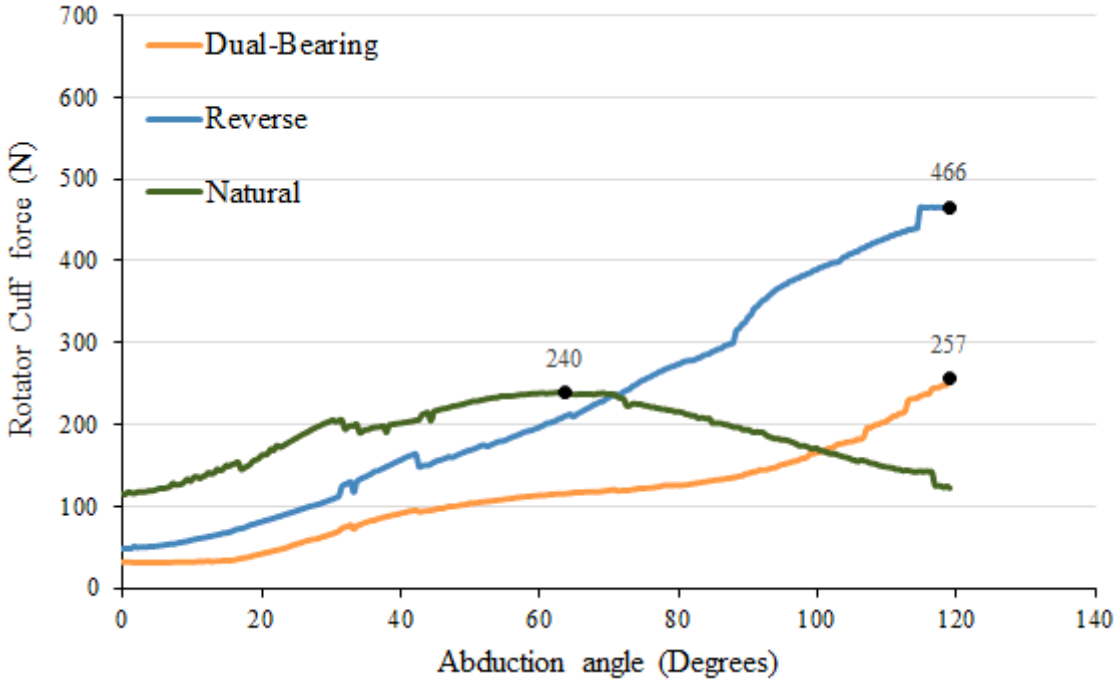

Figure 3

Rotator cuff muscle force vs abduction (ABD) angle for different shoulder models

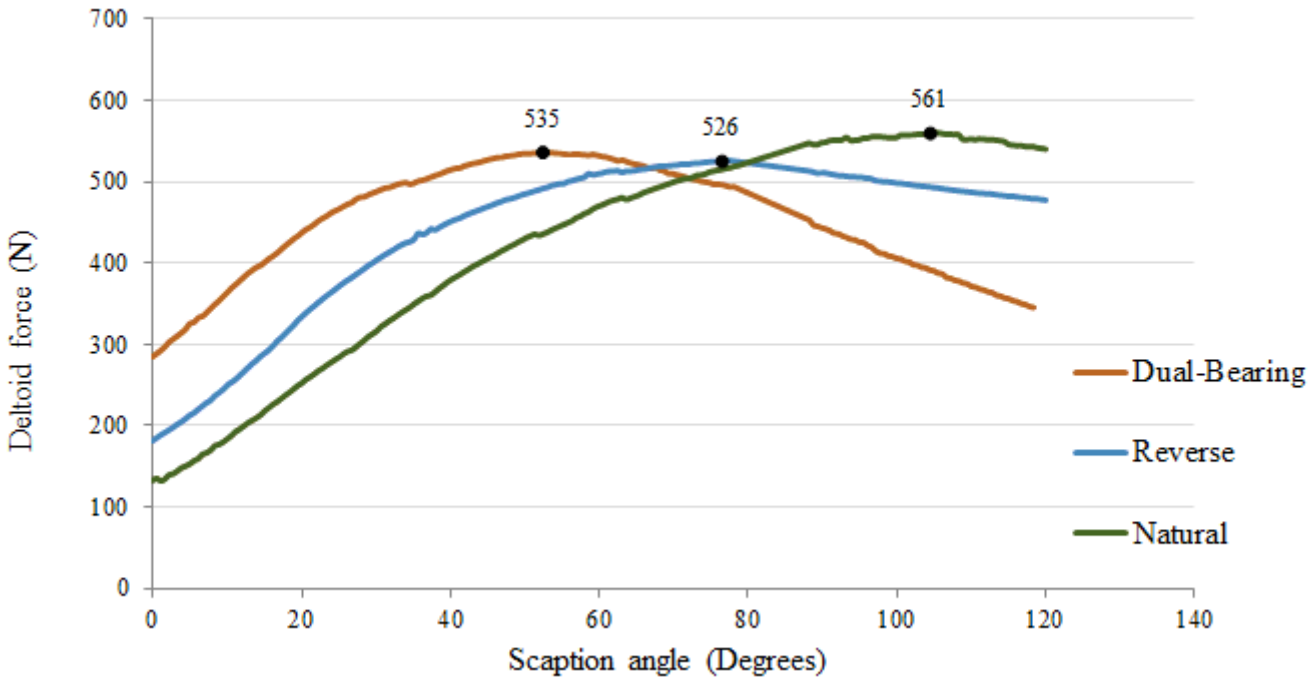

Figure 4

Deltoid muscle force vs scaption (SCP) angle for different shoulder models

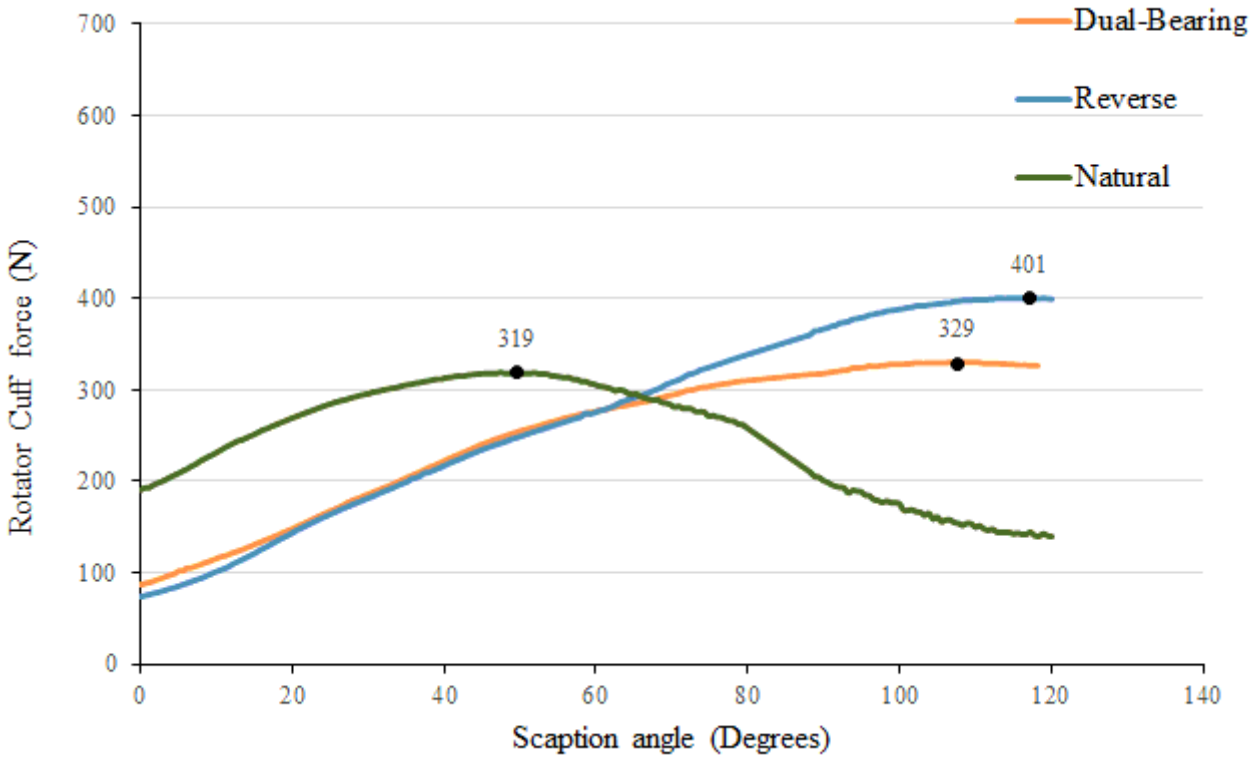

Figure 5

Rotator cuff muscle force vs scaption (SCP) angle for different shoulder models

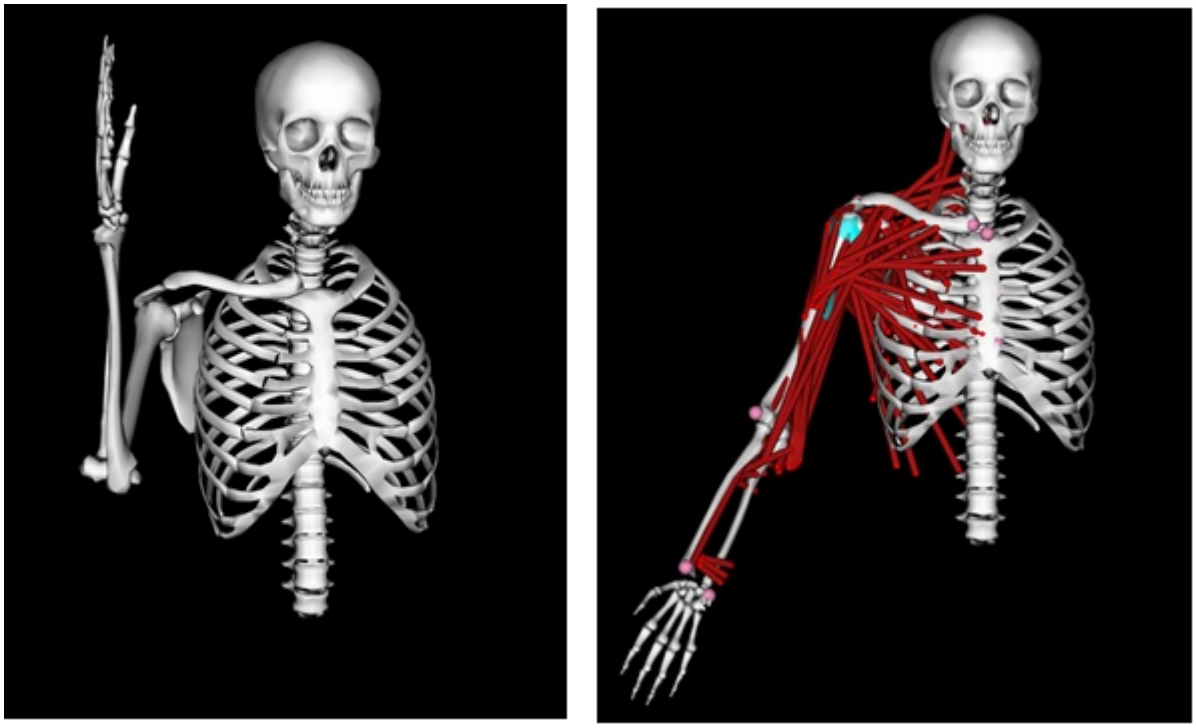

Figure 6

OpenSim® shoulder model incorporating the shoulder joint complex with all involved muscles (red), markers on bony landmarks (pink) and wrapping surface in humerus for the muscles (blue), (Left). Initial position of internal rotation at 60° of forward flexion (Right).

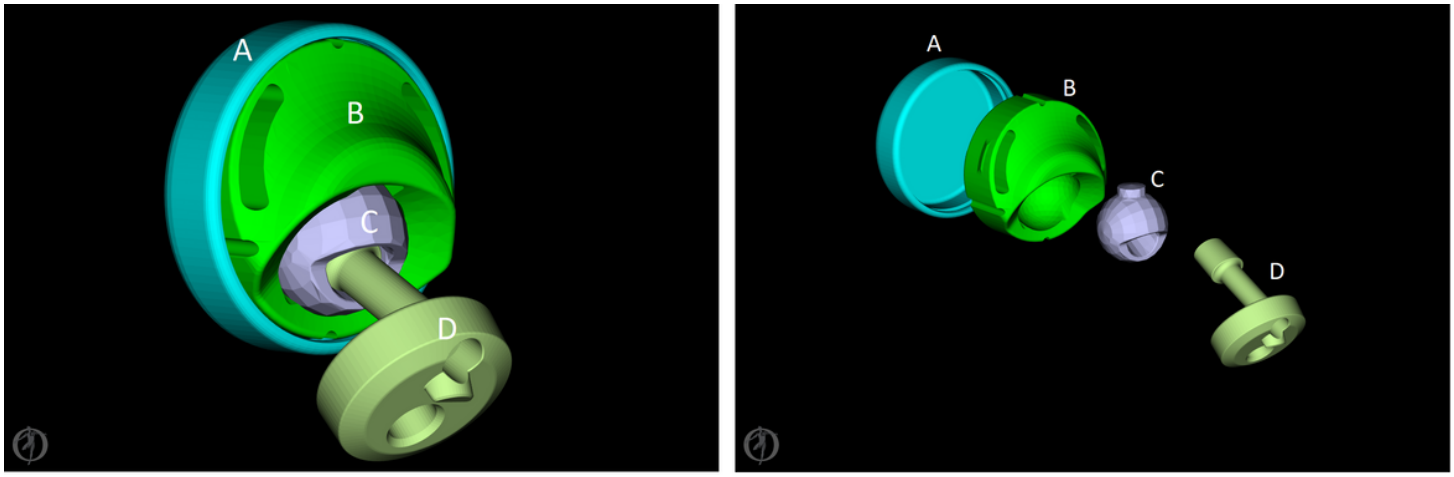

Figure 7

Principal components of the dual-bearing prosthesis: glenoid ring (A), PE-bearing (B); ball head (C); and offset adapter (D) of the dual-bearing prosthesis.

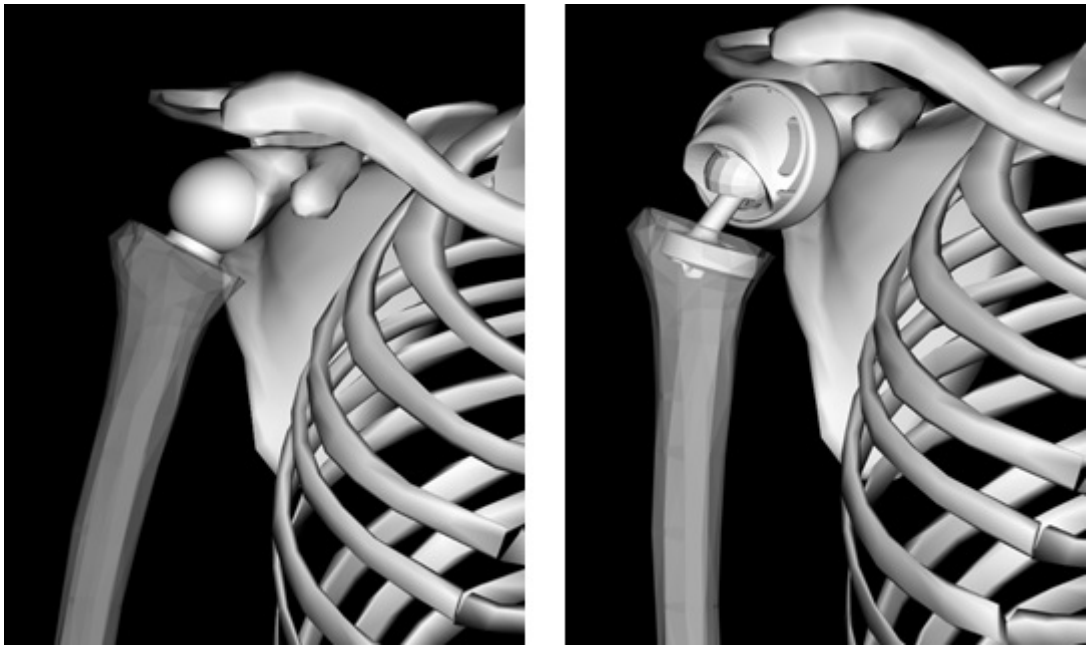

Figure 8

Dual-bearing shoulder prosthesis integrated in the model (left), Reverse shoulder prosthesis in the model (right).

Supplementary Files

This is a list of supplementary files associated with this preprint. Click to download.

- TableI.tif
- TableII.tif